

Bloch-Lorentz magnetoresistance oscillations in delafossites

K. Vilkelis^{1*, 2}, L. Wang^{2†}, A. Akhmerov²

1 Qutech, Delft University of Technology, Delft 2600 GA, The Netherlands

2 Kavli Institute of Nanoscience, Delft University of Technology, Delft 2600 GA, The Netherlands

† Current Address: Department of Physics, University of Konstanz, D-78457 Konstanz, Germany

* kostasvilkelis@gmail.com

September 22, 2022

Abstract

Recent measurements of the out-of-plane magnetoresistance of delafossites (PdCoO₂ and PtCoO₂) observed oscillations closely resembling the Aharonov-Bohm effect. Here, we show that the magnetoresistance oscillations are explained by the Bloch-like oscillations of the out-of-plane electron trajectories. We develop a semiclassical theory of these Bloch-Lorentz oscillations and show that they are a consequence of the ballistic motion and quasi-2D dispersion of delafossites. Our model identifies the sample wall scattering to be the most likely factor limiting the visibility of these Bloch-Lorentz oscillations in existing experiments.

Contents

1	Introduction	1
2	Ballistic in-plane model in the weak out-of-plane coupling limit	3
3	Results	5
3.1	Large Aspect Ratio Limit	5
3.2	Realistic sample geometry	7
3.3	Out-of-plane magnetic field	10
4	Summary	10
	References	11

1 Introduction

Known since the discovery of mineral CuFeO₂ by Friedel in 1873, delafossites are materials with the general formula ABO₂ [1, 2]. Delafossites are naturally occurring layered structures of alternating conductive A layer and insulating BO₂ layer with the overall $R\bar{3}m$

space group [3]. These materials are considered to be 2D owing to their weak interlayer coupling which results in a nearly cylindrical Fermi surface [4,5]. Of particular interest are PdCoO₂ and PtCoO₂ which were first synthesized and characterized at room temperature in 1971 by Shannon *et al.* [2,3,6]. Even though nearly 50 years have passed since then, the area of research is still very active due to the delafossites' impressive electronic transport properties [7]. At room temperature, it was shown that the conductivity of PdCoO₂ is 2.6 μΩ cm, very close to that of elemental copper [8]. Part of the reason for such large conductivity is the high Fermi velocity $7.5 \times 10^5 \text{ m s}^{-1}$ [8]. Another reason is their exceptional mean-free path at 4 K which exceed 20 μm [8]. Such value of mean-free path is accredited mostly to anomalously clean nature of delafossites and orbital-momentum locking [9,10]. Overall, all of these properties of delafossites make them a good platform to study mesoscopic ballistic transport [11].

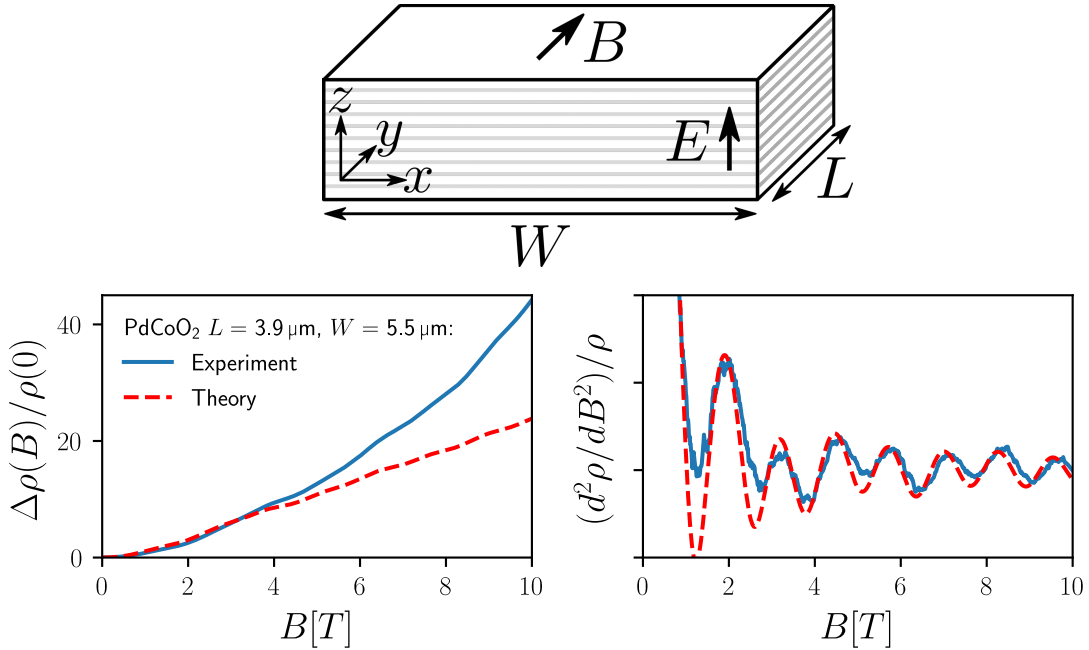


Figure 1: PdCoO₂ magnetoresistance experimental set up (top) and results (solid blue lines) obtained by Putzke *et al.* [12]. The semiclassical prediction (dashed red lines) was obtained by modeling the finite size PdCoO₂ sample.

Recent experiments studied the out-of-plane transport of PdCoO₂ [12], with the setup and the measured magnetoconductance shown in Fig. 1. Magnetoconductance was measured with the magnetic field applied in the plane of the delafossite layers and the current passing out-of-plane. Surprisingly, the results showed oscillations with a magnetic field similar to the Aharonov-Bohm effect. The period of the oscillations corresponded to adding a flux quantum through the area Wc with W the width of the sample and c the spacing between the adjacent conducting layers. These oscillations persisted up until 50 K, indicating the appreciable robustness of the phenomenon.

Simulations performed by Putzke *et al.* confirmed that the oscillations of Kubo conductivity with Aharonov-Bohm periodicity indeed appear in a minimal tight-binding model that combines high anisotropy with magnetic field [12]. While the theory [12] unambiguously demonstrated the phenomenon, it has the following limitations. This microscopic approach requires diagonalizing the Hamiltonian of the system and therefore it is prohibitively expensive to apply to real sample geometries—we will show below that the

sample geometry plays an important role. Furthermore, the role of different scattering mechanisms is not made clear. In particular, one may expect that strongly diffusive boundary scattering would suppress the Aharonov-Bohm like oscillations by removing closed trajectories. Finally, this microscopic approach does not exploit the large density of states in these materials, which motivates a semiclassical picture.

In this paper, we explain that the oscillations are a consequence of the shape of the semiclassical trajectories rather than an interference pattern. Our construction extends the idea put forward by Pippard [13] used to explain magnetoresistance oscillations in gallium [14]. Because our formalism does not rely on phase coherence, it is naturally compatible with the unusual robustness of the oscillations to temperatures as high as 50 K observed in Ref. [12]. The semiclassical approach also allows us to incorporate the appropriate bulk and boundary scattering rates, and simulate the full 2D cross-section of the sample. We conclude that the sample aspect ratio is the most likely factor limiting the visibility of the oscillations.

2 Ballistic in-plane model in the weak out-of-plane coupling limit

Delafossites' conduction band is well approximated by the energy dispersion

$$\varepsilon(\mathbf{k}) = \varepsilon_{\parallel}(\mathbf{k}_{\parallel}) - t_z \cos(k_z c'), \quad (1)$$

where $\varepsilon_{\parallel}(\mathbf{k}_{\parallel})$ is the in-plane dispersion relation with an approximately hexagonal Fermi surface [8,15,16], c' is the interlayer distance and t_z is the interlayer hopping. The interlayer dispersion is weak [4,8] i.e. t_z is much smaller than the in-plane bandwidth. This motivates a perturbative approach in terms of t_z that we use throughout the paper.

We compute electron density $f(\mathbf{r}, \mathbf{k}, t) d^3\mathbf{k}$ at position \mathbf{r} , time t and momentum \mathbf{k} by using the Boltzmann equation. We separate electron density into the equilibrium part and non-equilibrium parts:

$$f(\mathbf{r}, \mathbf{k}) = f^0 - g(\mathbf{r}, \mathbf{k}) \frac{\partial f^0}{\partial \varepsilon}, \quad (2)$$

where the equilibrium density f^0 (Fermi-Dirac distribution) becomes at zero temperature a Heaviside function so that its derivative $\frac{\partial f^0}{\partial \varepsilon}$ becomes a Dirac delta function centered around the Fermi energy. The resulting steady-state linearised Boltzmann equation [17] reads:

$$\mathbf{v} \cdot \nabla_{\mathbf{r}} g - \frac{e}{\hbar} (\mathbf{v} \times \mathbf{B}) \cdot \nabla_{\mathbf{k}} g - e v_z \mathcal{E}_z = \mathcal{L}g, \quad (3)$$

where \mathbf{v} is the velocity, e is the elementary charge, \hbar is the reduced Planck constant, \mathbf{B} is the magnetic field, \mathcal{E}_z is the electric field along the out-of-plane direction, and $\mathcal{L}g$ is the linearised collision integral. The boundary conditions at the boundary coordinate $\mathbf{r}_{\mathbf{B}}$ are

$$\begin{aligned} |\mathbf{v}(\mathbf{k}_{\parallel}) \cdot \hat{\mathbf{n}}_{\mathbf{B}}| g(\mathbf{r}_{\mathbf{B}}, \mathbf{k}) &= \int_{\mathbf{v}(\mathbf{k}'_{\parallel}) \cdot \hat{\mathbf{n}}_{\mathbf{B}} > 0} K(\mathbf{k}', \mathbf{k}) \times |\mathbf{v}(\mathbf{k}_{\parallel}) \cdot \hat{\mathbf{n}}_{\mathbf{B}}| g(\mathbf{r}_{\mathbf{B}}, \mathbf{k}') d^3k', \\ \mathbf{v}(\mathbf{k}_{\parallel}) \cdot \hat{\mathbf{n}}_{\mathbf{B}} &< 0. \end{aligned} \quad (4)$$

where $\hat{\mathbf{n}}_{\mathbf{B}}$ is the unit normal vector of the boundary (pointing inwards) and K is the boundary scattering kernel.

Utilizing the smallness of t_z , we expand g in Eq. (3) as a series to first order in t_z :

$$g(\mathbf{r}, \mathbf{k}) \approx g_0(\mathbf{r}, \mathbf{k}) + g_1(\mathbf{r}, \mathbf{k}), \quad (5)$$

where g_0 does not depend on t_z and $g_1 \propto t_z$. With the magnetic field inside the yz -plane $\mathbf{B} = (0, B_y, B_z)$, the zeroth-order expansion is

$$\mathbf{v}_{\parallel} \cdot \frac{\partial g_0}{\partial \mathbf{r}_{\parallel}} - \frac{e}{\hbar} (\mathbf{v}_{\parallel} \times \mathbf{B}) \cdot \nabla_{\mathbf{k}} g_0 = \mathcal{L}g_0, \quad (6)$$

where \mathbf{v}_{\parallel} is in-plane velocity. Equation (6) describes an electron in a magnetic field with no external forces capable of generating a steady non-equilibrium distribution. Under these conditions, non-zero scattering ensures that the steady state solution is $g_0 = 0$. Therefore, to first order in t_z linearised Boltzmann equation is

$$\mathbf{v}_{\parallel} \cdot \frac{\partial g}{\partial \mathbf{r}_{\parallel}} - \frac{e}{\hbar} (\mathbf{v}_{\parallel} \times \mathbf{B}) \cdot \nabla_{\mathbf{k}} g - ev_z \mathcal{E}_z = \mathcal{L}g. \quad (7)$$

Additionally, since $g \propto t_z$, it is sufficient to approximate \mathcal{L} to zeroth order in t_z .

Integrating Eq. (7) over k_z within the 1st Brillouin zone, we obtain an equation identical to Eq. (6), but with g_0 replaced by $g_{\parallel}(\mathbf{r}, \mathbf{k}_{\parallel}) \equiv \int_{\text{BZ}} g(\mathbf{r}, \mathbf{k}) dk'_z$. Therefore, the in-plane current of electrons vanishes in the steady state:

$$\int_{\text{BZ}} g(\mathbf{r}, \mathbf{k}) dk_z = 0. \quad (8)$$

We assume that the disorder in the bulk and at the boundaries is weakly correlated across the layers. Therefore, the disorder rapidly randomizes out-of-plane momentum k_z and leads to k_z -independent K and \mathcal{L} . The weakly correlated disorder together with Eq. (8) simplifies the linearised collision integral:

$$\mathcal{L}g = -\frac{g(\mathbf{k}_{\parallel}, k_z)}{\tau(\mathbf{k}_{\parallel})}, \quad (9)$$

where τ is the relaxation time which depends only on the in-plane wavevector \mathbf{k}_{\parallel} . Similarly, substitution of Eq. (8) in Eq. (4) and using the independence of K from k_z yields the simplified boundary conditions:

$$g(\mathbf{r}_{\mathbf{B}}, \mathbf{k}_{\parallel}, k_z) = 0, \text{ for } \mathbf{v}(\mathbf{k}_{\parallel}) \cdot \hat{\mathbf{n}}_{\mathbf{B}} < 0. \quad (10)$$

Neither the scattering Eq. (9) nor boundary conditions Eq. (10) mix non-equilibrium electron densities along different trajectories defined by the semiclassical equations of motion

$$\hbar \frac{d\mathbf{r}(t)}{dt} = \nabla_{\mathbf{k}} \varepsilon(\mathbf{k}), \quad \hbar \frac{d\mathbf{k}(t)}{dt} = -e\mathbf{v}(t) \times \mathbf{B}, \quad (11)$$

where t is the time along the trajectory. Therefore, using Eq. (11), we obtain the evolution of g along a single trajectory:

$$\frac{\partial g(t, \mathbf{r}_0, \mathbf{k}_0)}{\partial t} = \mathbf{v} \cdot \nabla_{\mathbf{r}} g - \frac{e}{\hbar} (\mathbf{v} \times \mathbf{B}) \cdot \nabla_{\mathbf{k}} g. \quad (12)$$

Here we parameterize each trajectory originating at a sample boundary through its initial coordinate and wave vector $\mathbf{r}_0 = (x_0, y_0, z_0)$ and $\mathbf{k}_0 = (k_0 \cos \theta_0, k_0 \sin \theta_0, k_{z,0})$. Substituting Eq. (12) and Eq. (9) into Eq. (7), we obtain the Boltzmann equation along a single trajectory

$$\frac{\partial g(t, \mathbf{r}_0, \mathbf{k}_0)}{\partial t} - e\mathcal{E}_z v_z(k_z(t)) = -\frac{g(t, \mathbf{r}_0, \mathbf{k}_0)}{\tau(\mathbf{k}_{\parallel}(t))}, \quad (13)$$

with solution

$$\begin{aligned} g(t, \mathbf{r}_0, \mathbf{k}_0) &= -e\mathcal{E}_z \int_0^t v_z(k_z(t')) \times \exp\left(-\frac{(t-t')}{\tau(\mathbf{k}_{\parallel}(t))}\right) dt' \\ &= -\frac{e\mathcal{E}_z t_z}{\hbar} \operatorname{Re} \left[\exp(ik_{z,0}) \int_0^t \exp(i\Delta k_z(t)) \times \exp\left(-\frac{(t-t')}{\tau(\mathbf{k}_{\parallel}(t))}\right) dt' \right], \end{aligned} \quad (14)$$

where $\Delta k_z(t)$ is the $k_z(t)$ solution to Eq. (11) with $k_z(0) = 0$ initial condition. Because $\Delta k_z(t)$ is fully determined by the in-plane trajectories, Eq. (14) shows that the excess electron distribution g is also fully determined by the in-plane trajectories.

To analyze experimental observations, we compute the current along z

$$I_{zz} = e \int_{S_{\parallel}} d^2 \mathbf{r}_{\parallel} \iint_{\text{BZ}} f(\mathbf{r}, \mathbf{k}) v_z(\mathbf{k}) d\mathbf{k}, \quad (15)$$

where the triple integral is over the 1st Brillouin zone, and S_{\parallel} is the in-plane surface area of the sample. We express the out-of-plane conductivity $\sigma_{zz} = I_{zz}/(S_{\parallel}\mathcal{E}_z)$ at zero temperature by substituting Eq. (2) into Eq. (15):

$$\sigma_{zz} = \frac{e}{S_{\parallel}\mathcal{E}_z} \int_{S_{\parallel}} d^2 \mathbf{r}_{\parallel} \iiint_{\text{BZ}} \delta(\varepsilon - \varepsilon_F) g(x, \mathbf{k}) v_z(\mathbf{k}) d\mathbf{k}, \quad (16)$$

where ε_F is the Fermi energy. In order to compute the lowest nonvanishing contribution in t_z to conductivity, we use $g_0 = 0$, and approximate the energy $\varepsilon(k_x, k_y, k_z) \approx \varepsilon_{\parallel}$ only to zeroth order in t_z . We switch to cylindrical coordinates in k -space (x, k, θ, k_z) where k is the in-plane wavevector length and θ is the azimuth. The conductivity to the lowest order in t_z is

$$\sigma_{zz} = \frac{e}{S_{\parallel}\mathcal{E}_z\hbar} \int_{S_{\parallel}} \int_0^{2\pi} \int_{-\frac{\pi}{c'}}^{\frac{\pi}{c'}} \frac{k_F(\theta)}{v_R(\theta)} g(x, k_F(\theta), \theta, k_z) \times v_z(k_z) d^2 \mathbf{r}_{\parallel} d\theta dk_z, \quad (17)$$

where

$$v_R(\theta) = \frac{1}{\hbar} \frac{\partial \varepsilon_{\parallel}}{\partial k}, \quad (18)$$

and $k_F(\theta)$ is the Fermi wavevector $\varepsilon(k_F(\theta), \theta) = \varepsilon_F$. We further simplify Eq. (17) by using that k_z enters Eq. (14) as a single complex exponent and carry out integration over k_z in a closed form.

3 Results

3.1 Large Aspect Ratio Limit

Because the mean free path of delafossites is larger than the sample size [12], to illustrate the origin of the oscillations we first neglect scattering $\mathcal{L}g = 0$. Furthermore, we assume the sample has a large aspect ratio $L/W \rightarrow \infty$ and therefore we utilize translational invariance of the sample along the y -direction. With in-plane magnetic field $\mathbf{B} = (0, B_y, 0)$, the Boltzmann Eq. (7) reduces to

$$v_x \frac{\partial g(x, v_x, k_z)}{\partial x} - v_x \frac{eB_y}{\hbar} \frac{\partial g(x, v_x, k_z)}{\partial k_z} - e\mathcal{E}_z v_z = 0. \quad (19)$$

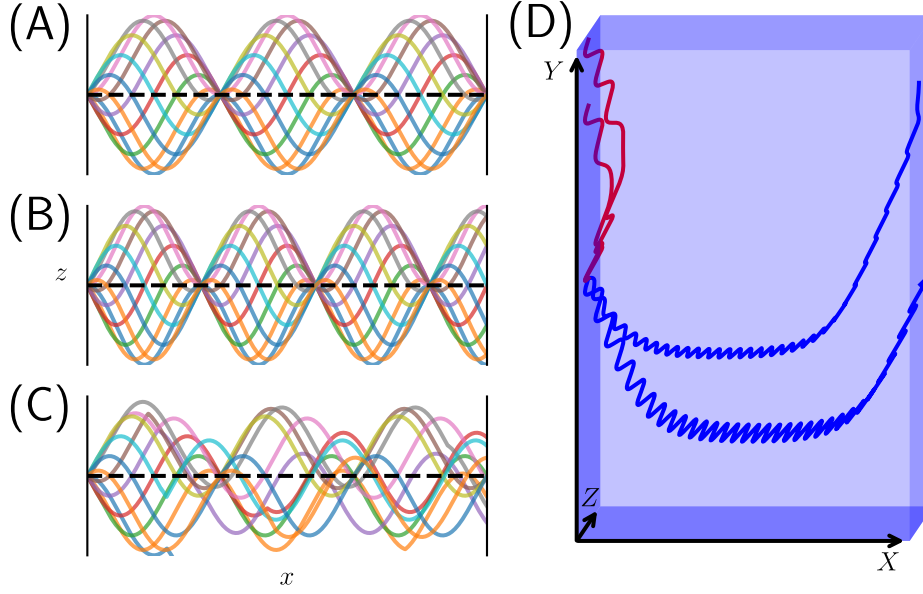


Figure 2: **(A)** Trajectories with oscillations commensurate to the sample width due to an in-plane magnetic field. Different curves indicate the different initial phases of the trajectory. **(B)** Same as in (A), but the in-plane magnetic field is chosen to give incommensurate oscillations. **(C)** Same as in (A), but with scattering present. **(D)** Trajectories due to an out-of-plane magnetic field. Blue lines are boundary-to-boundary trajectories whereas the red lines are edge-localized trajectories. Only the boundary-to-boundary trajectories produce current oscillations due to a net k_z drift throughout the trajectory.

In this simple limit, $g(x, v_x, k_z)$ only depends on k_x and k_y through $v_x(k_x, k_y)$. Solution to Eq. (19) fulfilling the boundary conditions of Eq. (10) is

$$g(x, v_x, k_z) = \frac{-t_z \mathcal{E}_z}{B_y v_x} \left[\cos(k_z c') - \cos\left(k_z c' + \frac{\omega B_y}{W} x_B\right) \right], \quad (20)$$

with:

$$\omega = \frac{e}{\hbar} c' W, \quad x_B = \begin{cases} x & \text{for } v_x > 0 \\ x - W & \text{for } v_x < 0. \end{cases} \quad (21)$$

We substitute Eq. (20) into Eq. (17), and obtain the conductivity along z

$$\sigma_{zz} = \frac{e\pi t_z^2}{\omega \hbar B_y^2} (1 - \cos(\omega B_y)) \int_0^{2\pi} \frac{k_F(\theta)}{v_x(\theta) v_R(\theta)} d\theta. \quad (22)$$

In other words, the conductivity has oscillations with an experimentally observed periodicity, but it vanishes in the minima so that the oscillations have a much larger amplitude.

To explain the large amplitude of the oscillations, we consider electron trajectories. When the magnetic field is of the form $\mathbf{B} = (0, B_y, B_z)$, the k_z dependence on x is

$$k_z(x) = k_{z0} + \frac{e}{\hbar} B_y x. \quad (23)$$

This ensures that all trajectories have a similar oscillatory vertical displacement as a function of x :

$$z(x) = \frac{t_z}{\hbar v_x} \left[\cos\left(k_{z0} + \frac{e}{\hbar} B_y x\right) - \cos(k_{z0}) \right]. \quad (24)$$

We plot the trajectories in Fig. 2(A, B). The universal trajectory shape is a result of the k_z advancing over the complete out-of-plane Brillouin zone, similar to Bloch oscillations [18], however, the origin of the momentum drift is Lorentz force instead of the electric field. This gives k_z a universal dependence on x regardless of the in-plane trajectory. When the oscillation period is commensurate with the sample width, all trajectories have a zero net vertical displacement over the time of flight, and therefore carry no current as shown in Fig. 2(A). At the same time, the vertical displacement of different trajectories—and therefore the current—is maximal when a half-integer number of oscillation periods fits into the sample width as shown in Fig. 2(B). Because the contribution of every trajectory to the conductance has the same magnetic field dependence, as seen in Eq. (22), this minimal model yields an oscillatory conductance with a correct frequency, but full visibility of the oscillations in contrast to the experimental data.

3.2 Realistic sample geometry

Bulk scattering cannot explain the disagreement between the experiment and the minimal model because the mean-free-path of $20\ \mu\text{m}$ [8] is much larger than the dimensions of samples used by Putzke *et al.* [12] ($4\ \mu\text{m}$ to $6\ \mu\text{m}$). Therefore, the dominant source of scattering must originate from the boundaries. In the experimental setup by Putzke *et al.* [12], the sample has a low aspect ratio with a sample length shorter than the width $W > L$. As a result, we expect the boundaries along the length of the sample to alter the semiclassical trajectories.

To analyse the effects of small aspect ratio, we consider a rectangular geometry with boundaries at: $x = 0$, $x = W$, $y = 0$, $y = L$. We parameterize the trajectories by their point of origin at the boundary and the initial angle θ_0 . At a sufficiently high out-of-plane magnetic field, bulk cyclotron orbits appear that do not intersect with sample boundaries. We disregard these trajectories because they do not contribute to the h/e magnetoresistance oscillations, however extending our approach to those trajectories is straightforward. By changing the variables in Eq. (17) to the trajectory coordinate system (t, θ_0, k_{z0}) , we bring σ_{zz} to the form

$$\sigma_{zz} = \frac{-e}{W\mathcal{E}_z\hbar} \oint dr_0 \int_{\theta_{min}}^{\theta_{max}} d\theta_0 \int_0^{t_B(\theta_0, \mathbf{r}_0)} dt' \frac{k_F(\theta(\theta_0, t'))}{v_R(\theta(\theta_0, t'))} J(t', \theta_0) \times \int_{-\pi/c}^{\pi/c} dk_{z0} g(\mathbf{r}_0, t', \theta_0, k_{z0}) v_z(\mathbf{r}_0, t', \theta_0, k_{z0}), \quad (25)$$

with the Jacobian determinant:

$$J(t', \theta_0) = \left(\frac{\partial \theta}{\partial t'} \Big|_{t'=0} \right)^{-1} \frac{\partial \theta}{\partial t'} v_x(0, \theta_0). \quad (26)$$

In Eq. (25), the r_0 integral is over the sample boundary and $t_B(\theta)$ is the time that the trajectory hits a boundary. The integral over θ_0 includes the contributions of all trajectories within the sample.

We solve Eq. (25) numerically with an in-plane magnetic field B_y and without bulk scattering $\tau \rightarrow \infty$. The results in Fig. 3 left panel shows the oscillations decaying with decreasing aspect ratio L/W of the sample. The visibility of the oscillations drops with a lower aspect ratio due to more trajectories scattering off the sample side-boundaries. Using the geometry of the sample of Ref. [12], we confirm that the computed relative magnitude

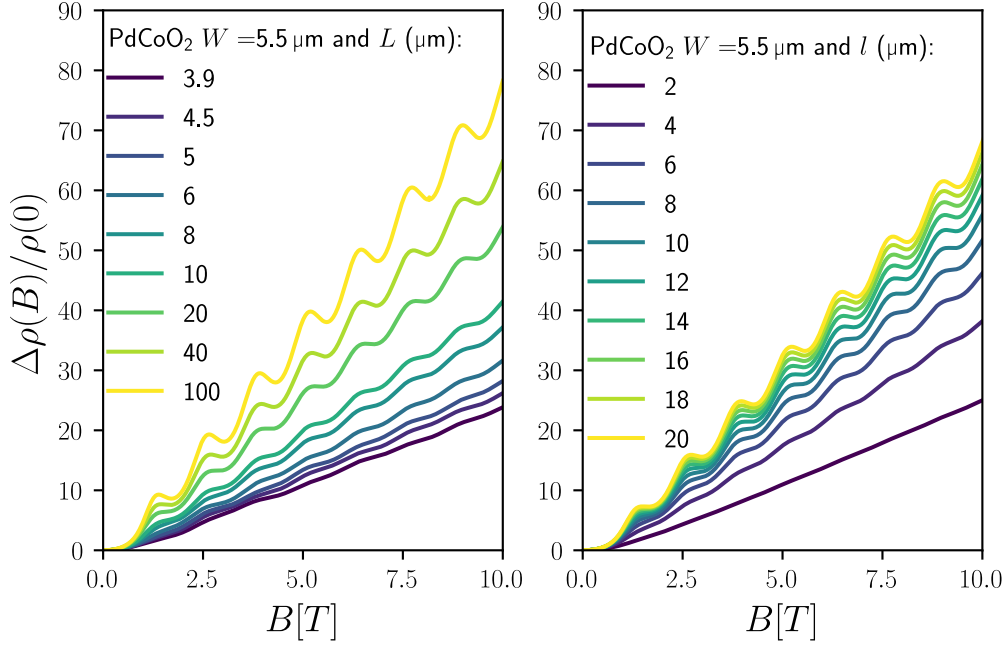


Figure 3: (Left panel) Semiclassical predictions of PdCoO₂ magnetoresistance with variable sample aspect ratio and no bulk scattering. (Right Panel) Semiclassical predictions of PdCoO₂ magnetoresistance sample with translational invariance along y and variable bulk scattering (mean-free-path l).

of the oscillations agrees with the measured values, however, the overall resistance profile is somewhat different, as shown in Fig. 1. The possible reasons for this disagreement are residual bulk scattering, minor misalignment of the magnetic field, or inhomogeneity of the sample along the z -direction.

The scattering from the side-boundaries plays a similar role to bulk disorder. To demonstrate this, we apply the theory in the high aspect ratio limit in Eq. (19) to include bulk scattering through Eq. (9). The solution to the resulting linearised Boltzmann equation with relaxation is

$$g(x, \theta, k_z) = \frac{\mathcal{E}_z \tau e c' t_z}{\hbar (B_y^2 \phi^2 + 1)} \left(B_y \phi \cos(k_z c') + \sin(k_z c') - \exp\left(-\frac{x_B}{l}\right) \left[B_y \phi \cos\left(k_z c' + \frac{\omega B_y}{W} x_B\right) + \sin\left(k_z c' + \frac{\omega B_y}{W} x_B\right) \right] \right), \quad (27)$$

with

$$l(\theta) = \tau v_x(\theta), \quad \phi(\theta) = \frac{e}{\hbar} c' l(\theta). \quad (28)$$

Here we assume that τ is constant along the Fermi surface. We substitute Eq. (27) into Eq. (17), and obtain conductivity per unit azimuth

$$\sigma_{zz}(B_y) = \frac{\tau e^2 t_z^2 c' \pi}{\hbar^2} \int_0^{2\pi} \frac{k_F(\theta)}{v_R(\theta) (B_y^2 \phi^2 + 1)^2} \times \left(1 - r + (B_y \phi)^2 r + (B_y \phi)^2 + r \exp\left(-\frac{1}{r(\theta)}\right) \times \left[(1 - B_y^2 \phi^2) \cos(\omega B_y) - 2 B_y \phi \sin(\omega B_y) \right] \right) d\theta, \quad r \equiv l(\theta)/W. \quad (29)$$

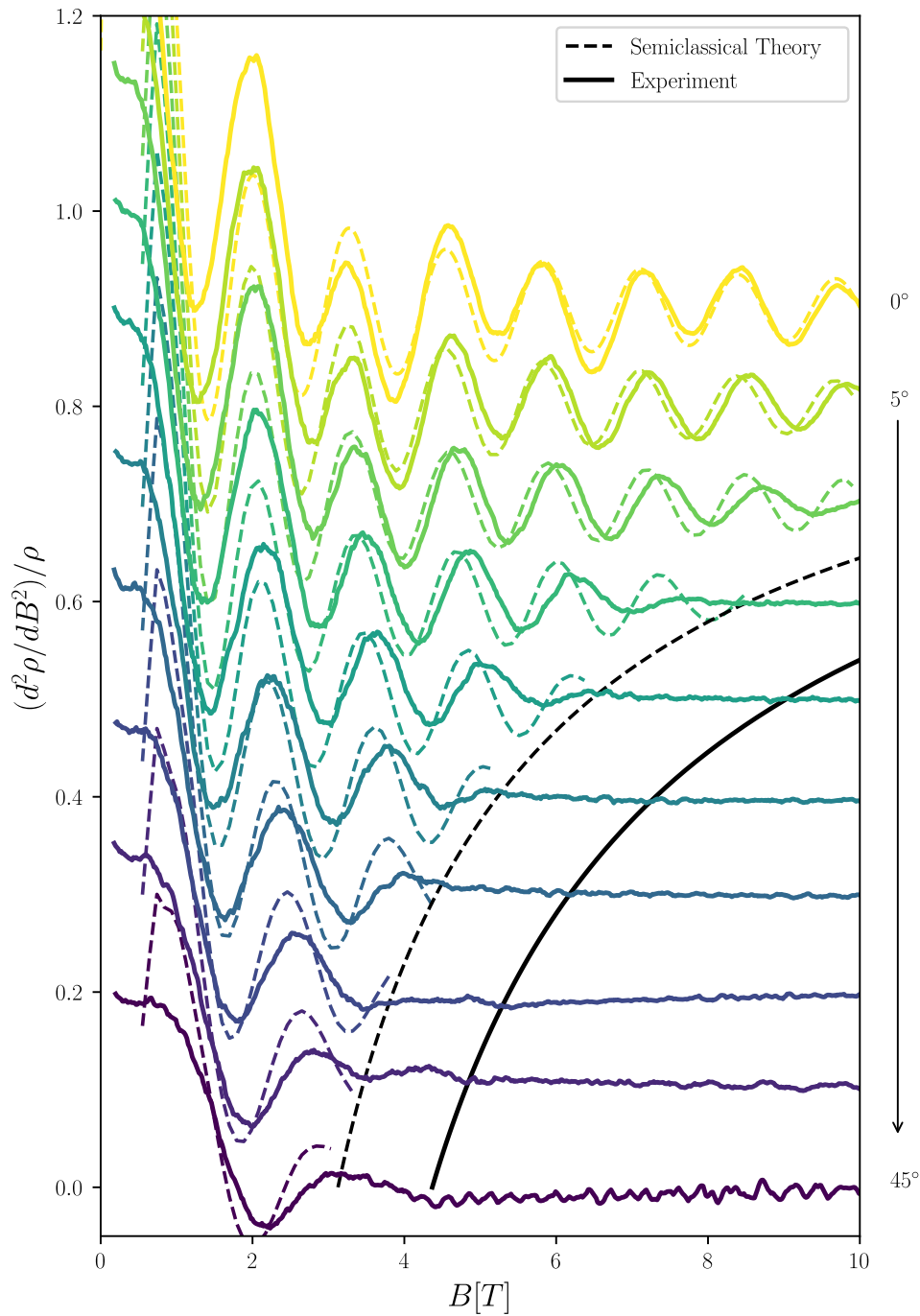


Figure 4: Numerical results from the semiclassical theory (dashed lines) with $l(0) = 4.4 \mu\text{m}$ compared to the experimental (solid lines) magnetoresistance results by Putzke *et al.* [12] for magnetic field tilted out-of-plane by 5° steps. Black lines indicate the critical field when the cyclotron orbit fits inside the sample. The critical field value is determined by the shorter side of the sample. In the experiment, this is the length of the sample L , whereas in the semiclassical prediction it is the width of the sample W .

We recover a simple Drude model B^2 resistivity scaling [19] in Eq. (29) by removing the boundaries, $W \rightarrow \infty$, which removes the second term in Eq. (29). The results of Eq. (29)

for various values of mean-free-path l are shown in the right panel of Fig. 3. We observe that the scattering of the side boundaries in a sample with a finite aspect ratio results in a similar magnetoresistance as bulk scattering. Moreover, our simulations show that the magnitude of the oscillations due to side boundary scattering in the geometry used in the experiment is comparable to the observed one (see Fig. 1). Based on this we conclude that the sample aspect ratio is the factor likely limiting the oscillation visibility in the experiment.

3.3 Out-of-plane magnetic field

In the presence of an out-of-plane magnetic field B_z , the in-plane projection of each trajectory is a rotated and rescaled hexagonal Fermi surface, while the out-of-plane motion follows the oscillatory pattern of Eq. (24) (see Fig. 2(D)). We use the integral form of the Boltzmann Eq. (25) to find the magnetoresistance response. To reduce the numerical cost required to evaluate a 4D integral of Eq. (25), we approximate the side boundary scattering by using a finite relaxation time τ instead. We expect that this approximation, while somewhat crude, should capture the essential physics, as supported by the comparison between the two mechanisms shown in Fig. 3. To evaluate the remaining 3D integral, we choose the starting point of each trajectory as $t = 0$, so that its initial conditions are $\mathbf{r}_0 = (x_0, y_0, z_0)$ and $\mathbf{k}_0 = (k_0 \cos \theta_0, k_0 \sin \theta_0, k_{z,0})$. Here $x_0 = 0$ and $-\pi/2 < \theta_0 < \pi/2$ at the left boundary, while $x_0 = W$ and $\pi/2 > \theta_0 > 3\pi/2$ at the right boundary.

In presence of the out-of-plane magnetic field, some trajectories cross from one boundary to the opposite, while others return to the boundary from which they originated, as shown in Fig. 2(D). Only the trajectories that cross the sample contribute to the conductance oscillations because they have a net k_z drift given by Eq. (23). On the other hand, the trajectories returning to the boundary where they originated do not contribute to the oscillations. As Putzke *et al.* [12] pointed out, once the cyclotron orbits become smaller than W , which happens at

$$B_z > \left(\frac{2\hbar k_F}{eW} \right), \quad (30)$$

with k_F the Fermi wavevector, ballistic trajectories crossing the sample disappear, and so do the conductance oscillations.

We perform numerical integration of Eq.(25), with the result shown in Fig. 4. The model qualitatively agrees with the experimental data at the small tilt angles from the xy -plane. However, the disagreement increases with B_z , likely due to our calculation approximating side boundary scattering with a constant relaxation time. This is likely a crude approximation because the sample length L is shorter than W in the experiment. The extension of the theory to a realistic sample geometry is straightforward—especially since one may still compute g for every trajectory independently—but it strongly increases the computational costs, and therefore we consider it unjustified for our study.

4 Summary

In summary, we demonstrated that the observed magnetoresistance of delafossite materials is explained by the Bloch-like oscillations of the out-of-plane electron trajectories. These Bloch-Lorentz oscillations arise from the quasi-2D dispersion of these materials combined with the nearly ballistic motion of the electrons. We identify the sample aspect ratio as the most likely factor limiting the oscillation visibility. modeling achieves a qualitative agreement with the experiment without introducing any free parameters.

Acknowledgements

We would like to thank Ady Stern, Veronika Sunko, and Maja Bachmann for the helpful discussions in the early stages of the project. Special thanks to Carlo Beenakker for his valuable feedback and advice on the manuscript. Also, we are grateful to Philip J.W. Moll and Carsten Putzke for sharing with us their experimental findings and subsequent consultations.

Data Availability

All code and data used in the manuscript are available at Ref. [20].

Author contributions

A.A. formulated the project idea. K.V. developed the theory, carried out numerical simulations, and analyzed the data with input from the other authors. The manuscript was written jointly by K.V. and A.A. with input from L.W.

Funding information

This work was supported by the NWO VIDI Grant (016.Vidi.189.180), an ERC Starting Grant 638760, and European Union's Horizon 2020 research and innovation programme FE-TOpen Grant No. 828948 (AndQC).

References

- [1] C. Friedel, *Sur une combinaison naturelle des oxydes de fer et de cuivre, et sur la reproduction de l'atacamite*, Sciences Academy **77**, 211 (1873).
- [2] R. D. Shannon, D. B. Rogers and C. T. Prewitt, *Chemistry of noble metal oxides. i. syntheses and properties of abO_2 delafossite compounds*, Inorganic Chemistry **10**(4), 713 (1971).
- [3] R. D. Shannon, C. T. Prewitt and D. B. Rogers, *Chemistry of noble metal oxides. ii. crystal structures of platinum cobalt dioxide, palladium cobalt dioxide, copper iron dioxide, and silver iron dioxide*, Inorganic Chemistry **10**(4), 719 (1971).
- [4] K. P. Ong, J. Zhang, J. S. Tse and P. Wu, *Origin of anisotropy and metallic behavior in delafossite $PdCoO_2$* , Phys. Rev. B **81**, 115120 (2010), doi:[10.1103/PhysRevB.81.115120](https://doi.org/10.1103/PhysRevB.81.115120).
- [5] H.-J. Noh, J. Jeong, J. Jeong, E.-J. Cho, S. B. Kim, K. Kim, B. I. Min and H.-D. Kim, *Anisotropic electric conductivity of delafossite $PdCoO_2$ studied by angle-resolved photoemission spectroscopy*, Phys. Rev. Lett. **102**, 256404 (2009), doi:[10.1103/PhysRevLett.102.256404](https://doi.org/10.1103/PhysRevLett.102.256404).
- [6] R. D. Shannon, D. B. Rogers, C. T. Prewitt and J. L. Gillson, *Chemistry of noble metal oxides. iii. electrical transport properties and crystal chemistry of abO_2 compounds with the delafossite structure*, Inorganic Chemistry **10**(4), 723 (1971).
- [7] A. P. Mackenzie, *The properties of ultrapure delafossite metals*, Reports on Progress in Physics **80**(3), 032501 (2017), doi:[10.1088/1361-6633/aa50e5](https://doi.org/10.1088/1361-6633/aa50e5).

- [8] C. W. Hicks, A. S. Gibbs, A. P. Mackenzie, H. Takatsu, Y. Maeno and E. A. Yelland, *Quantum oscillations and high carrier mobility in the delafossite PdCoO_2* , Physical Review Letters **109**(11) (2012), doi:[10.1103/physrevlett.109.116401](https://doi.org/10.1103/physrevlett.109.116401).
- [9] V. Sunko, P. McGuinness, C. Chang, E. Zhakina, S. Khim, C. Dreyer, M. Konczykowski, H. Borrmann, P. Moll, M. König and et al., *Controlled introduction of defects to delafossite metals by electron irradiation*, Physical Review X **10**(2) (2020), doi:[10.1103/physrevx.10.021018](https://doi.org/10.1103/physrevx.10.021018).
- [10] H. Usui, M. Ochi, S. Kitamura, T. Oka, D. Ogura, H. Rosner, M. W. Haverkort, V. Sunko, P. D. C. King, A. P. Mackenzie and K. Kuroki, *Hidden kagome-lattice picture and origin of high conductivity in delafossite PtCoO_2* , Phys. Rev. Materials **3**, 045002 (2019), doi:[10.1103/PhysRevMaterials.3.045002](https://doi.org/10.1103/PhysRevMaterials.3.045002).
- [11] M. D. Bachmann, A. L. Sharpe, A. W. Barnard, C. Putzke, M. König, S. Khim, D. Goldhaber-Gordon, A. P. Mackenzie and P. J. W. Moll, *Super-geometric electron focusing on the hexagonal fermi surface of PdCoO_2* , Nature Communications **10**(1) (2019), doi:[10.1038/s41467-019-13020-9](https://doi.org/10.1038/s41467-019-13020-9).
- [12] C. Putzke, M. D. Bachmann, P. McGuinness, E. Zhakina, V. Sunko, M. Konczykowski, T. Oka, R. Moessner, A. Stern, M. König, S. Khim, A. P. Mackenzie et al., *h/e oscillations in interlayer transport of delafossites* (2019), [1902.07331](https://arxiv.org/abs/1902.07331).
- [13] A. B. Pippard, *Magnetomorphic oscillations due to open orbits*, The Philosophical Magazine: A Journal of Theoretical Experimental and Applied Physics **13**(126), 1143 (1966), doi:[10.1080/14786436608213529](https://doi.org/10.1080/14786436608213529), <https://doi.org/10.1080/14786436608213529>.
- [14] J. A. Munarin and J. A. Marcus, *New oscillatory magnetoresistance effect in gallium*, In J. G. Daunt, D. O. Edwards, F. J. Milford and M. Yaqub, eds., *Low Temperature Physics LT9*, pp. 743–747. Springer US, Boston, MA, ISBN 978-1-4899-6443-4 (1965).
- [15] H. Takatsu, J. J. Ishikawa, S. Yonezawa, H. Yoshino, T. Shishidou, T. Oguchi, K. Murata and Y. Maeno, *Extremely large magnetoresistance in the nonmagnetic metal PdCoO_2* , Phys. Rev. Lett. **111**, 056601 (2013), doi:[10.1103/PhysRevLett.111.056601](https://doi.org/10.1103/PhysRevLett.111.056601).
- [16] J. C. A. Prentice and A. I. Coldea, *Modeling the angle-dependent magnetoresistance oscillations of fermi surfaces with hexagonal symmetry*, Phys. Rev. B **93**, 245105 (2016), doi:[10.1103/PhysRevB.93.245105](https://doi.org/10.1103/PhysRevB.93.245105).
- [17] J. M. Ziman, *Principles of the Theory of Solids*, Cambridge University Press, ISBN 9780521297332, doi:[10.1017/CBO9781139644075](https://doi.org/10.1017/CBO9781139644075) (1972).
- [18] F. Bloch, *Über die quantenmechanik der elektronen in kristallgittern*, Zeitschrift für physik **52**(7-8), 555 (1929).
- [19] S. Zhang, Q. Wu, Y. Liu and O. V. Yazyev, *Magnetoresistance from fermi surface topology*, Phys. Rev. B **99**, 035142 (2019), doi:[10.1103/PhysRevB.99.035142](https://doi.org/10.1103/PhysRevB.99.035142).
- [20] K. Vilkelis and A. Akhmerov, *Bloch-Lorentz magnetoresistance oscillations in delafossites*, doi:[10.5281/zenodo.4977422](https://doi.org/10.5281/zenodo.4977422), This work was supported by the NWO VIDI Grant (016.Vidi.189.180), an ERC Starting Grant 638760 and European Union’s Horizon 2020 research and innovation programme FE-TOpen Grant No. 828948 (AndQC). (2020).